Optical Materials 179 (2026) 118365

Contents lists available at ScienceDirect

Optical Materials

journal homepage: www.elsevier.com/locate/optmat

Research Article

Investigating the Dy^{3+}→Tb^{3+} energy transfer dynamics in YAG ceramics and crystals

Angela Pirri [a,*], Andrea Lapini [b], Jiang Li [c,d], Tingsong Li [c,d], Lexiang Wu [c], Yiyang Liu [c], Martin Nikl [e], Jan Pejchal [e], Akira Yoshikawa [f], Guido Toci [g], Leonida A. Gizzi [h], Enrico Cavalli [i]

[a] Istituto di Fisica Applicata "N. Carrara", Consiglio Nazionale delle Ricerche, CNR-IFAC, Via Madonna del Piano 10C, Sesto Fiorentino (Fi), 50019, Italy
[b] Department of Chemical Sciences, Life and Environmental Sustainability, University of Parma, Parco Area delle Scienze, 11/a, Parma, 43124, Italy
[c] State Key Laboratory of High Performance Ceramics, Shanghai Institute of Ceramics, Chinese Academy of Sciences, Shanghai, 201899, China
[d] Center of Materials Science and Optoelectronics Engineering, University of Chinese Academy of Sciences, Beijing, 100049, China
[e] Institute of Physics of the Academy of Sciences of the Czech Republic, Cukrovarnicka 10, Prague, 162 00, Czech Republic
[f] Institute for Materials Research, Tohoku University, 2-1-1 Katahira, Sendai, 980-8577, Japan
[g] Istituto Nazionale di Ottica, Consiglio Nazionale delle Ricerche, CNR-INO, Via G. Moruzzi 1, Pisa, 56124, Italy
[h] Istituto Nazionale di Ottica, Consiglio Nazionale delle Ricerche, CNR-INO, Via Madonna del Piano 10C, Sesto Fiorentino (Fi), 50019, Italy
[i] Chemical Physics at the Department of Chemical Sciences, Life and Environmental Sustainability, University of Parma, Parco Area delle Scienze, 11/a, Parma, 43124, Italy

ARTICLE INFO

Keywords:
Dysprosium
Terbium
Energy transfer
Yellow laser

ABSTRACT

A detailed study of the emission dynamics in high-optical-quality YAG ceramics singly and co-doped with Dy^{3+} and Tb^{3+} has been carried out in order to investigate the energy transfer processes between the two ions which may influence the potential of (Dy,Tb):YAG as a yellow laser medium. The excited state dynamics of Dy^{3+} and Tb^{3+} were studied at room temperature under different experimental conditions to confirm the positive effect of the Tb^{3+} co-doping on the Dy^{3+} $^4F_{9/2}$ → $^6H_{13/2}$ yellow emission channel. Finally, the results obtained in YAG ceramics were compared to those obtained in YAG crystals grown by the μ-pulling down method with the same Dy^{3+} and Tb^{3+} co-doping levels.

1. Introduction

In the last decade the research on optical lasers has been driven by matrices (in ceramics or single-crystal form) doped with rare-earth ions directly emitting in the visible region [1–6] and excited by commercial laser-diode sources. In particular, the $^4F_{9/2}$ → $^6H_{13/2}$ transition around 575-580 nm (depending on the host) of Dy^{3+} has been considered attractive for yellow laser applications [1,7,8]. However, there are factors strongly affecting the efficiency of this transition:

- the low values of the emission and absorption cross-sections in the visible range (due to their spin-forbidden nature) [9,10];
- concentration dependent quenching mechanisms;
- the long decay time of the final $^6H_{13/2}$ level of the transition of interest, which leads to population bottlenecking.

All these factors can be optimized as they depend on the nature and the optical quality of the host matrix, the doping level, the operating conditions, and so on. In particular, the lifetime or radiative time (τ_{rad}), of an excited state is an intrinsic characteristic associated to its oscillator strength. The effective decay time is usually shorter than the lifetime, since the excited level can relax also 'via' non-radiative mechanisms, namely multiphonon relaxation (MPR) and energy transfer (ET) processes. The former mechanism is dependent on the host, in particular on its optical phonon energy, and in general its direct effect on the emission properties in the visible region is rather limited, but it can favour some thermally assisted energy transfer mechanisms important for achieving laser action. The energy transfer processes are strongly dependent on the interactions between the doping ions and can have positive or negative effect on the performance of a given emission channel. In particular, it is known that the yellow emission of Dy^{3+} is subject to concentration quenching at relatively low doping levels [7,9], and that its performance

* Corresponding author.
E-mail address: angela.pirri@cnr.it (A. Pirri).

https://doi.org/10.1016/j.optmat.2026.118365
Received 13 May 2026; Received in revised form 26 June 2026; Accepted 23 July 2026
Available online 23 July 2026
0925-3467/© 2026 The Authors. Published by Elsevier B.V. This is an open access article under the CC BY license (http://creativecommons.org/licenses/by/4.0/).

can be significantly improved by co-doping with Tb^{3+}, thanks to the efficient $(Dy^{3+})^6H_{13/2} \rightarrow (Tb^{3+})^7F_4$ energy-transfer mechanism [9–17], that depopulates the $^6H_{13/2}$ final level of the transition. We have recently investigated this process in (Dy^{3+},Tb^{3+}):LuAG ceramics [18] and confirmed its potentiality in favouring the efficiency of the yellow laser channel.

This paper is devoted to the study of the excited states dynamics of Dy, Tb^{3+}:YAG systems in both ceramic and crystalline forms. We have investigated the emission properties of co-doped (Dy(x*at.%*),Tb(y*at.%*)): YAG ceramics and single crystals (with x = 3 or 5, y = 0.5 or 1 with respect to Y^{3+}) as well as those of single-doped 3 *at%*Dy:YAG and 1 *at%* Tb:YAG ceramics as comparison terms. The systematic analysis of the experimental data provides useful information for evaluating the suitability of the investigated materials for yellow solid-state laser applications.

2. Experimental

2.1. Synthesis and characterization of ceramics

In the present study, α-Al_2O_3 (99.99%), Y_2O_3 (99.999%), Dy_2O_3 (99.99%), Tb_4O_7 (99.99%), MgO (99.99%) and tetraethoxysilane (TEOS, 99.999%) were used as starting materials. The raw powders mixed with TEOS and MgO were milled in ethanol for 12 h using 10 mm diameter alumina balls as the milling medium. After ball milling, the slurry was dried, uniaxially pressed into 20 mm diameter pellets at 40 MPa, and then cold isostatically pressed at 250 MPa. Then the green compacts were pre-sintered under vacuum at 1700°C for 5 h and then HIP post-treated at 1650°C in an argon atmosphere of 180 MPa for 3 h. Finally, the obtained transparent ceramics were air annealed at 1400°C for 10 h to eliminate oxygen vacancies and then were mirror-polished into 1.2 mm for further characterizations. The X-ray diffraction (XRD, D8 Advance, Bruker, Germany) was performed to determine the phase composition of the prepared ceramics. The morphologies of thermally etched surfaces of the ceramics were observed by the field emission scanning electron microscopy (FESEM, SU8220, Hitachi, Japan). The in-line transmittance spectra of mirror-polished ceramics were measured by a UV-VIS-NIR spectrophotometer (Cary-5000, Varian, USA).

Fig. 1(a) and (b) shows the XRD patterns of the (Dy,Tb):YAG ceramics and magnified inset around the dominant 420 peak at 2θ~33.3°. The comparison with the standard YAG pattern (PDF#33-0040) confirms the formation of the target garnet phase, even if in the cases of the lowest and highest Dy, Tb doping concentrations the presence of some additional phase cannot be excluded.

FESEM micrographs of HIP post-treated Dy,Tb:YAG ceramics are shown in Fig. 2. All samples are pore-free and the microstructures are qualitatively consistent, that is, grain shapes are similar in all samples regardless of composition. However, as the doping amount of Dy and Tb gradually increases, the grain size of the ceramic increases accordingly. On the one hand, both ionic radii of Tb^{3+} (approximately 1.04 Å) and Dy^{3+} (approximately 1.03 Å) are larger than that of Y^{3+} (approximately 1.02 Å). When they replace Y^{3+} in the crystal lattice, they can induce local lattice distortions. Moreover, the increase in doping content produces an increase in the concentration of lattice defects, which provides more channels for ion migration, thereby significantly enhancing grain boundary mobility. The faster the grain boundary moves, the more rapidly the grains grow.

Photos and in-line transmission spectra of the polished (Dy,Tb):YAG ceramics are shown in Fig. 3. All the samples are transparent, even if to different extent, as shown in Fig. 3(a). The differences in transparency are an effect of the optical scattering, the ceramics being constituted by grains with different sizes and defectiveness and are responsible for the different baselines observed in the transmission spectra of Fig. 3(b). For the rest, the spectra show the typical absorption bands of the doping ions, with intensities in line with the corresponding concentration levels. Features ascribable to the eventual presence of additional phase

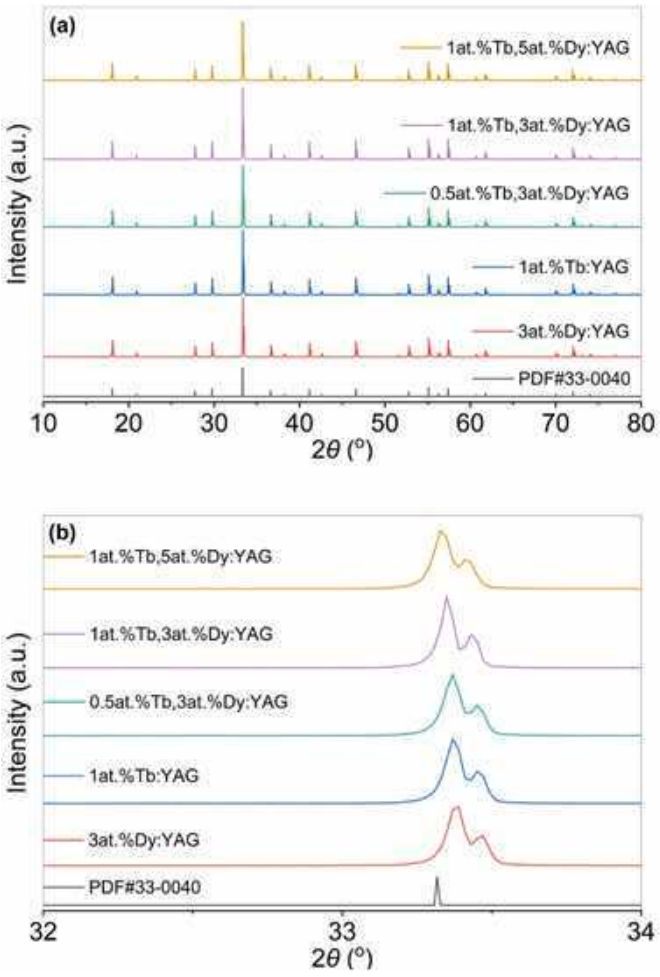


Fig. 1. (a) XRD patterns of Dy,Tb:YAG ceramics pre-sintered at 1700°C for 5h in vacuum and HIP post-treated at 1650°C for 3 h under 180 MPa in Ar; (b) Magnified inset around the dominant 420 peak at 2θ~33.3°.

are not detectable, and this allows us to reliably investigate the emission dynamics of the materials.

2.2. Crystals growth and characterization

The (Dy,Tb)-doped YAG crystals were grown by micro-pulling-down (μ-PD) method [19,20] with radiofrequency inductive heating from the corresponding stoichiometric mixtures of 4 N purity Y_2O_3, Al_2O_3, Dy_2O_3 and Tb_4O_7 oxides from Stella Chemifa Co., Japan. The growth was performed using an iridium crucible with a die of 2 mm in diameter and nozzle diameter of 0.5 mm under N_2 (4 N) atmosphere using <111> oriented Czochralski-grown YAG single crystal as a seed (provided by Crytur Co. Ltd. Czech Republic). The crucible was placed on an iridium after heater with windows and on alumina pedestal. The hot zone around the crucible consisted of 3 layers of alumina shielding for thermal insulation. The N_2 gas flow was kept at 0.5 l/min. The crucible with the starting materials was heated up to the YAG melting temperature, which is around 1970°C. Then, the YAG single-crystal seed was brought into contact with the melt coming through the nozzle due to the capillary action. The pulling speed was 0.1 mm/min.

The as-gown crystal rods had diameter of 2 mm and were around 60-70 mm in length, without visible cracks or inclusions, as shown in Fig. 4. The samples were cut from the crystal in the form of circular platelets and mirror-polished to the thickness of 1 mm.

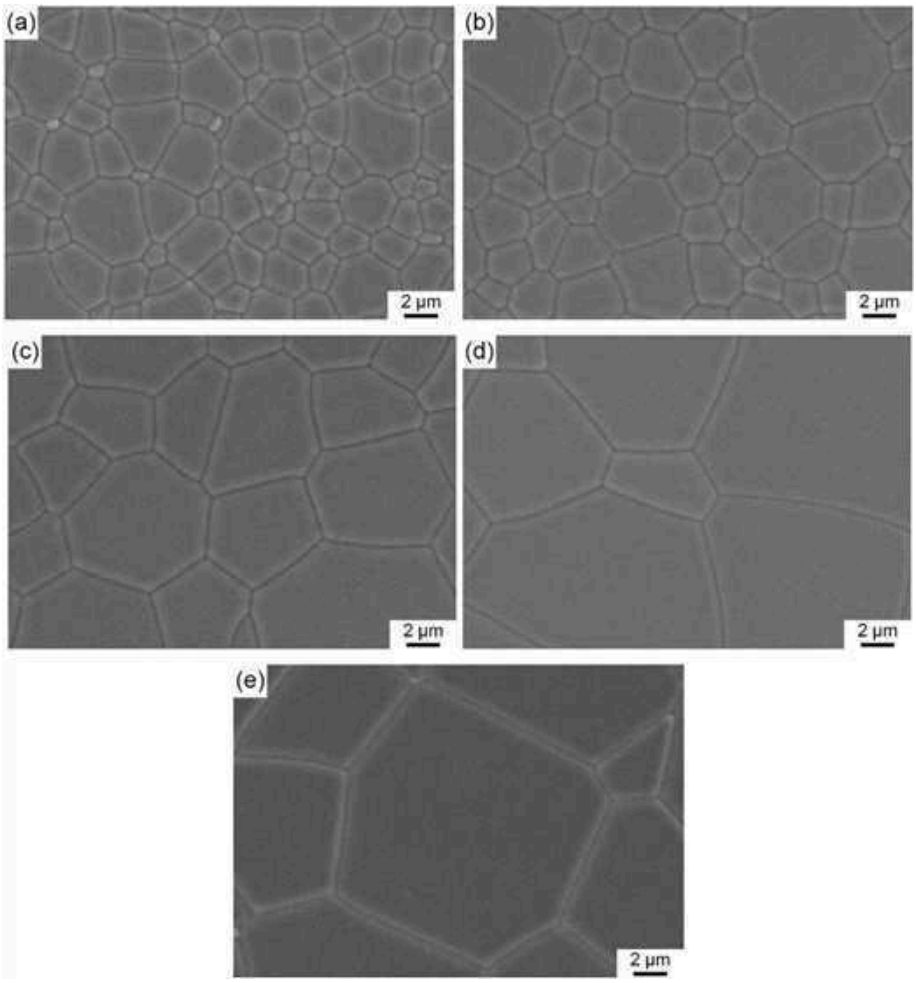


Fig. 2. FESEM micrographs of the fracture surfaces and thermally etched surface of HIP post-treated Dy,Tb:YAGceramics: (a) 3 *at*%Dy:YAG; (b) 1 *at*%Tb:YAG; (c) (3 *at*%Dy, 0.5 *at*%Tb):YAG; (d) (3 *at*%Dy,1 *at*%Tb):YAG; (e) (5 *at*%Dy,1 *at*%Tb):YAG.

2.3. Spectroscopic characterization

The emission and excitation spectra as well as the luminescence decay curves were measured at room temperature using an Edinburgh FLS1000 spectrophotometer, with a resolution of 0.1 nm.

Different mathematical models have been used for the fit of the experimental decay profiles, depending on their characteristics (presence of a faster initial trend, of a rising component, composition of the sample under investigation, etc.) by paying attention to the literature data concerning similar materials, when available, in order to obtain the most accurate information possible on the relaxation dynamics of the investigated systems.

3. Results

3.1. Dy(3 at.%):YAG and Tb(1 at.%):YAG ceramics

The spectroscopic characterization of the Dy(3 at.%):YAG ceramic is reported in Fig. 5, together with the energy levels scheme of Dy^{3+} (Fig. 5 (a)) [5], useful for the assignment of the observed transitions. The excitation spectrum, Fig. 5(b), was measured in correspondence of the most intense emission line at 575 nm. The observed manifolds have been assigned according to literature data [21].

The emission spectra, reported in Fig. 5(c), have been measured upon excitation at $\lambda_{exc} = 353$ and $\lambda_{exc} = 386$ nm, in correspondence of two different excitation manifolds of Dy^{3+} (see Fig. 5(b)) in order to verify if there are effects attributable to site distortions, indicating some crystal defectiveness. Apart the intensity, the two spectra are well resolved and practically identical, confirming the excellent optical quality of the sample. Four band systems are present, assigned to the transitions from the $^4F_{3/2}$ energy level to the $^6H_{15/2}$ ($\lambda_{em} = 480$ nm), $^6H_{13/2}$ ($\lambda_{em} = 575$ nm), $^6H_{11/2}$ ($\lambda_{em} = 675$ nm) and $^6H_{9/2} + {}^6F_{11/2}$ ($\lambda_{em} = 760$ nm). The CIE coordinates of the emission have been measured (0.33, 0.35) and are in proximity to the standard white point (0.33, 0.33).

The emission decay curve (Fig. 5(d)) is non-exponential, as a consequence of energy transfer processes between the Dy^{3+} ions. According to the literature concerning analogous materials [22] and to its profile, having a faster initial component, it has been reproduced using the Inokuti-Hirayama model (Eq. (1)), assuming a dipole-dipole interaction. The fit is in good agreement with the experimental data ($R^2 = 0.9997$).

$$\phi(t) = A \cdot \exp\left[-\frac{t}{\tau} - \alpha \left(\frac{t}{\tau_{rad}} \right)^{3/s} \right] \quad (1)$$

$\phi(t)$ is the emission intensity after the pulse, A is the emission intensity at t = 0, τ_{rad} is the lifetime of the isolated ion, and s is the multipolar interaction parameter, having value 6 for dipole-dipole (D-D) interaction. The decay profile has been reproduced by considering A, τ, and α as adjustable parameters. The obtained values are A = 1.04, $\alpha = 1.474$ and $\tau_{rad} = 0.99$ ms. The radiative lifetime is consistent with that calculated by some authors through the Judd-Ofelt analysis of the absorption spectra [23,24], but much longer than that evaluated by

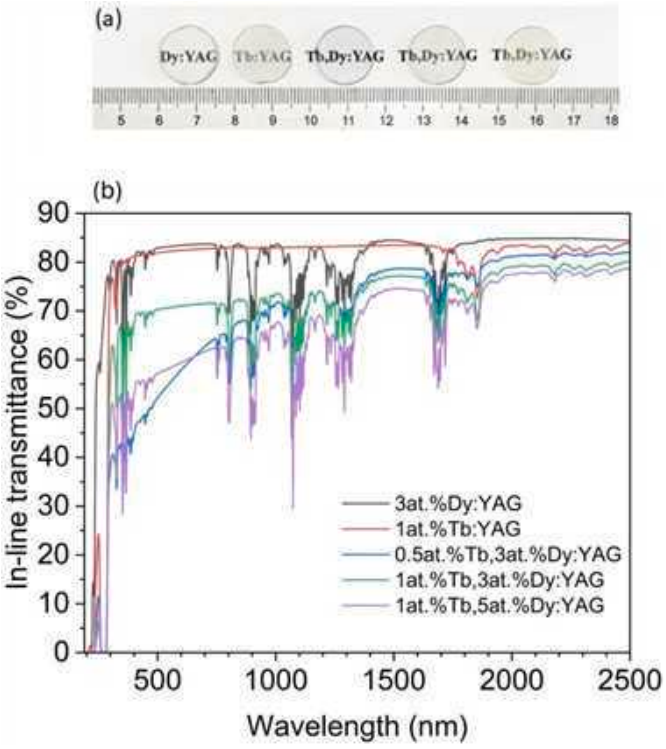


Fig. 3. Photographs (a) and in-line transmittance spectra (b) of HIP post-treated (Dy,Tb):YAG ceramics.



Fig. 4. Micro-pulling-down grown crystal of (3 *at*%Dy,1 *at*%Tb):YAG.

integrating the normalized profile, τ_{aver} = 0.35 ms, attesting that the energy transfer processes strongly affect the quantum efficiency of the material. Measurements carried out using an integrating sphere report a 20% value for the quantum efficiency of a similar material [21]. The parameter α provides information on the probability of the transfer process:

$$\alpha = \frac{4}{3}\pi\Gamma\left(1-\frac{3}{s}\right)N_a R_0^3 \tag{2}$$

where Γ is the gamma function, N_a the doping concentration in ions·cm^{-3}, and R_0 is the critical distance of the transfer process. Knowing the α value, with this equation it is possible to estimate R_0. In the present study the resulting value is 7.8 Å, which is in good agreement with the minimum distance of 8.3 Å between the Dy^{3+}-Dy^{3+}, calculated on the basis of the structural data and of the doping concentration.

Several mechanisms are involved in the energy transfer process, in particular the cross-relaxations:

$$^4F_{9/2} + {}^6H_{15/2} \rightarrow (^6F_{3/2}, {}^6F_{1/2}) + (^6H_{9/2}, {}^6F_{11/2}) \tag{3}$$

$$^4F_{9/2} + {}^6H_{15/2} \rightarrow (^6H_{9/2}, {}^6F_{11/2}) + (^6F_{3/2}, {}^6F_{1/2})$$

as shown in Fig. 5(a). These mechanisms are nearly resonant and responsible for the significant concentration quenching usually observed in the Dy^{3+} doped materials [7,25].

The spectroscopic characterization of the 1 *at*%Tb:YAG ceramic is reported in Fig. 6. As in the previous case, the spectra have been interpreted with the help of the energy levels scheme of the Tb^{3+} ion (Fig. 6(a)) [26]. The excitation spectrum (Fig. 6(b)) has been measured in correspondence of the intense emission line at 543 nm. The most intense excitation features consist of broadbands at 285 nm and 324 nm assigned to *f-d* transitions. The much weaker *f-f* transitions are shown in the inset of Fig. 6(b), evidencing the positions of the $^5D_3$ and $^5D_4$ emitting levels (around 377 and 480 nm, respectively). In particular, at the adopted concentration level (*i.e.* 1 *at*%), the $^5D_4$ level is efficiently populated by the $^5D_3$ one through the resonant cross-relaxation process [27,28]:

$$^5D_3, {}^7F_6 \rightarrow {}^5D_4, {}^7F_1 \tag{4}$$

that is schematically represented by the dashed lines in Fig. 6(a). For this reason, the emission spectrum (Fig. 6(c)) is dominated by the transitions from the $^5D_4$ state, the $^5D_4 \rightarrow {}^7F_5$ one at 543 nm being the most intense and at the origin of the green colour of the Tb^{3+} luminescence. The spectrum has been excited at 354 nm, in correspondence of the $^5D_2$ level. The emission from the $^5D_3$ level is strongly quenched by the cross-relaxation process, and only some weak bands are observable in the 400-480 nm region of the spectrum. The intensity of the band in the 420 nm region was, however, sufficient for the measurement of the decay profile (Fig. 6(d)), useful to investigate the nature of the cross-relaxation process. It can be reliably reproduced by the Inokuti-Hirayama model (see Eq. (1)) considering a dipole-dipole interaction. The best fit (R^2 = 0.9995) was obtained with A = 1.05, α = 1.850 and τ_{rad} = 1.49 ms, a value not far from that (τ_{rad} = 1.65 ms) reported by Bodenschatz et al. for a single crystal [29]. The average decay time evaluated by integration of the normalized curve is 0.34 ms, attesting that the cross relaxation strongly affects the quantum efficiency of the $^5D_3$ level. The critical distance of the transfer process, R_0, estimated using Eq. (2), is 12.2 Å, practically coincident with the minimal medium distance between the Dy^{3+} doping ions, 12.0 Å. The decay profile of the $^5D_4$ emission is shown in Fig. 6(e). It exhibits an initial rising component, consequence of the above cited cross-relaxation process (Eq. (4)). The most adequate model for its analysis is the difference of exponentials function (Eq. (5)), that allows to estimate both decay time and population rate of the emitting state:

$$\phi(t) = A_1 \cdot \exp\left(-\frac{t}{\tau_{dec}}\right) - A_2 \cdot \exp\left(-\frac{t}{\tau_{rise}}\right) \tag{5}$$

The resulting rise time, τ_{rise} = 0.25 ms, is comparable with the integrated decay time of the $^5D_3$ level, particularly when considering the steep slope of the initial segment of the curve in Fig. 6(d). The decay time of the $^5D_4$ emission is τ_{dec} = 3.24 ms.

As specified in the introduction section, the singly doped systems have been investigated to provide a comparison in the study of the co-doped materials. We have tried to verify their agreement with previous literature on these compounds, in particular for what concerns the decay time values, and realized that the amount of data available is very large and often discordant, because there are different factors affecting their performances. A discussion on this aspect would require a detailed analysis that is out of the scope of this paper.

3.2. *(Dy(xat.%), Tb(yat.%)):YAG ceramic with (x = 3, 5; y = 0, 0.5, 1)*

The initial part of this section is focused on the spectroscopy of the (Dy(3 *at*%), Tb(0.5 *at*%)):YAG ceramic, since it provides elements useful for the interpretation of all experimental data. The emission spectra measured upon Tb^{3+} (λ_{exc} = 315 nm) and Dy^{3+} (λ_{exc} = 447 nm) excitation are shown in Fig. 7(a). The 447 nm excitation wavelength allows to exclude any concomitance with the excitation lines of Tb^{3+}, based on the excitation spectra of Fig. 6(b). In the former case the Tb^{3+} emission is obviously prevalent with respect to that of Dy^{3+}, but some of its main features are visible around 489 and 580 nm, superimposed to the Tb^{3+} manifolds, and also at.

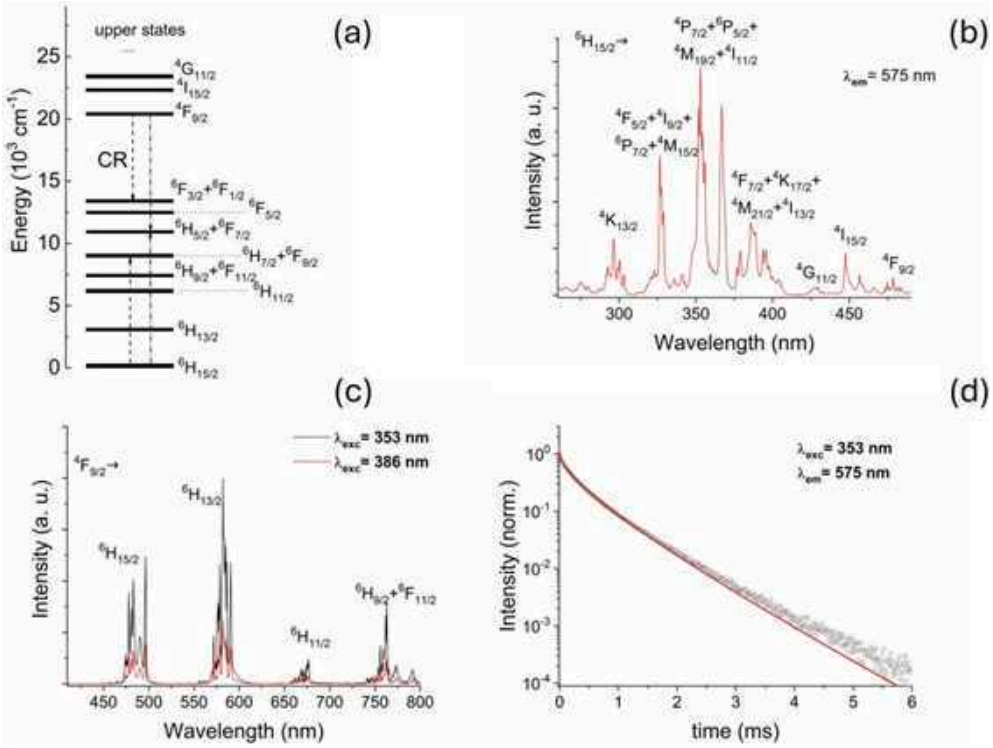


Fig. 5. (a) Energy levels scheme of Dy^{3+} and cross-relaxation processes involving the $^4F_{9/2}$ level. (b) Excitation spectrum of 3 *at*%Dy^{3+}: YAG ceramic. (c) Emission spectra; (d) Decay profile, the red line being the fit of the experimental data using Eq. (1). (For interpretation of the references to colour in this figure legend, the reader is referred to the Web version of this article.)

760 nm. In the latter case, although the Dy^{3+} luminescence is predominant, some Tb^{3+} emission features are clearly observable in the 550 nm and 620 nm regions. In conclusion, in this material there are both $Dy^{3+}\rightarrow Tb^{3+}$ and $Tb^{3+}\rightarrow Dy^{3+}$ energy transfer processes, depending on the excitation conditions. The excitation spectra as reported in Fig. 7 (b) confirm this situation. The spectrum of the Tb^{3+} emission at $\lambda_{em} = 543$ nm (black line) is very similar to that of the singly doped system (Fig. 6(b)), the main difference being in some reabsorption dips around 330 nm and in a very weak excitation feature at 490 nm, both ascribable to the presence of Dy^{3+}. The spectrum measured by observing the Dy^{3+} emission at $\lambda_{em} = 582$ nm (red line) in the 325-500 nm range is practically identical to that of the singly doped ceramics, whereas below 325 nm are well evident the *f-d* Tb^{3+} transitions, rather weak in consideration of their nature of allowed transitions, attesting, however, the presence of the $Tb^{3+}\rightarrow Dy^{3+}$ transfer.

The possible energy transfer processes between the Dy^{3+} and Tb^{3+} ions are illustrated in Fig. 8: the transfer from the *f-d* states of Tb^{3+} to Dy^{3+} are indicated with ETD_{fd}, whereas that from Dy^{3+} to Tb^{3+} in the visible range originates only from the $^4F_{9/2}$ level and is indicated with EDT1.

The Dy^{3+} decay profile has been measured in correspondence of the $\lambda_{em} = 763$ nm emission upon direct Dy^{3+}(404 nm) excitation in order to exclude any contribution of Tb^{3+}, both in excitation and in emission, and also upon Tb^{3+} ($\lambda_{exc} = 270$ nm) excitation (see Fig. 9(a)), in order to investigate the nature of the $Tb^{3+}\rightarrow Dy^{3+}$ transfer. Both decays are strongly non-exponential and cannot be analysed using simple models; only an average estimation of the decay time can be obtained by integration of the normalized curves. The value obtained in the 404 nm excitation case, $\tau_{aver} = 0.36$ ms, is practically identical to that observed for 3 *at*%Dy:YAG (0.35 ms): this means that the Dy^{3+}-Dy^{3+} interaction (concentration quenching) strongly prevails over the (Dy^{3+}) $^6H_{13/2}\rightarrow$(Tb^{3+}) $^7F_4$ energy transfer (see ETD2 in Fig. 8). This is important, because this latter mechanism is considered a favorable condition for achieving visible laser action [9–18]: it is then of fundamental importance to optimize the relative concentrations of the two active ions in order to achieve the highest emission efficiency. The decay time of Dy^{3+} excited 'via' $Tb^{3+}\rightarrow Dy^{3+}$ transfer is much longer, 1.13 ms (integrated decay time), similar to the lifetime of the $^4F_{9/2}$ state evaluated using the Judd-Ofelt Theory, around 1 ms [6,7]. In order to account for this behavior, we suppose that there can be an interaction between the final states of the involved emission transitions: in particular, a resonant energy transfer from the $^7F_4$ of Tb^{3+}, populated 'via' the 587 nm emission, to the $^6H_{13/2}$ level of Dy^{3+} (see ETD2 in Fig. 8). Once populated, this state relaxes to the $^6H_{15/2}$ ground state rather slowly in consequence of its relatively long decay time (usually 2-3 ms), inducing consequently a significant slowing of the radiative depopulation of the $^4F_{9/2}$ excited state.

The emission curves of the $^5D_3$ level of Tb^{3+} have not been measured because the transitions from this level were too weak for reliable measurements. The decay profile of the $^5D_4$ emission is shown in Fig. 9(b): the rise time associated the $^5D_3$-$^5D_4$ cross relaxation is barely visible (roughly of the order of 40-50 μs) in consequence of the long distance between the Tb^{3+} ions, due to the low concentration. Another possible reason could be connected to a shortening of the $^5D_3$ decay time induced by the resonant energy transfer towards the $^4P_{3/2}$, $^6P_{5/2}$ levels of the Dy^{3+} ions (ETD1 in Fig. 8), a mechanism whose probability appears greater with respect to that of the $^5D_3$-$^5D_4$ cross relaxation, in consideration of the fact that the Tb–Dy distance is much shorter than the Tb–Tb one. For the rest the profile is nearly a single exponential with decay time of $\tau_{dec} = 2.54$ ms, shorter than that of the singly doped ceramic (3.24 ms). We suppose that this is because this state transfers energy to the Dy^{3+} ions 'via' the nearly resonant, and then rather efficient, (Tb^{3+}) $^5D_4\rightarrow$ (Dy^{3+}) $^4F_{9/2}$ mechanism indicated with ETD2 in Fig. 8.

The emission spectra of all co-doped system excited at 447 nm (Dy^{3+}) are collected in Fig. 10. The Dy^{3+} emission intensity does not vary significantly when the Tb^{3+} concentration increases from 0.5 *at*% to 1 *at* % and its emission intensity increases. When the dysprosium

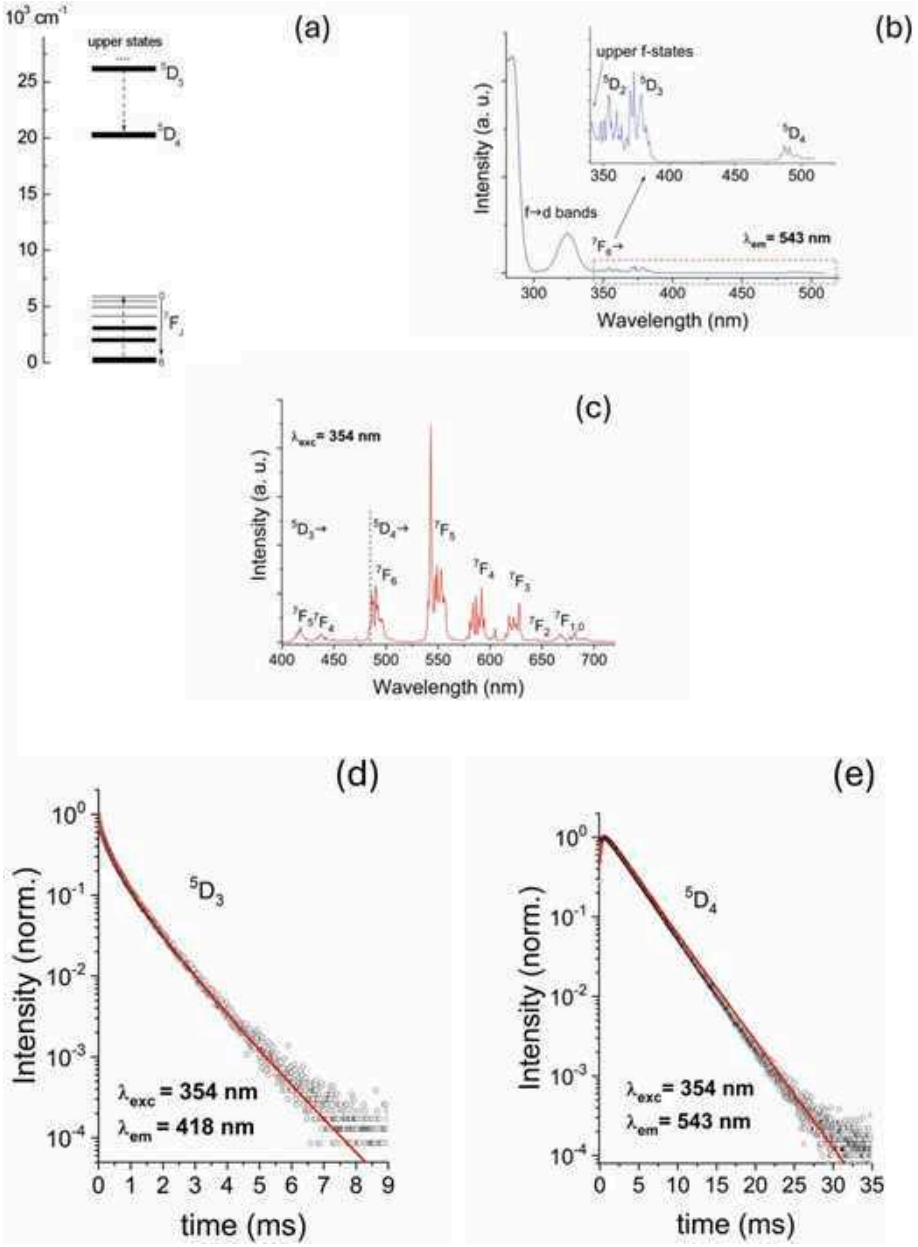


Fig. 6. (a) Energy levels scheme of Tb^{3+} and cross-relaxation processes involving the $^5D_3$ level; (b) Excitation spectrum of 1 *at*%Tb:YAG ceramic; (c) Emission spectra; (d) Decay profile of the $^5D_3$ level, the red line being the fit of the experimental data using Eq. (1); (e) Decay profile of the $^5D_3$ level, the red line being the fit of the experimental data using Eq. (5). (For interpretation of the references to colour in this figure legend, the reader is referred to the Web version of this article.)

concentration changes from 3 *at*%Dy^{3+} to 5 *at*%Dy^{3+} (with 1 *at*%Tb^{3+}) the intensity of the whole spectrum decreases in consequence of the concentration quenching mechanisms mentioned in the previous section (see Eq. (3)). However, the ratio between the intensities of the Tb^{3+} with respect to the Dy^{3+} bands is the same as in (Dy(3 *at*%), Tb(0.5 *at*%)):YAG, despite the Dy–Tb distance (as well as the Dy–Dy one) is significantly shorter. On this basis we can conclude that the cross-relaxation mechanisms (see Eq. (3)) tend to prevail over the interactions of Dy^{3+} with Tb^{3+}, dominating the emission dynamics of the system.

Fig. 11 compares the excitation spectra of the $^4F_{9/2}$ emission in 3 *at*% Dy^{3+}:YAG and (3 *at*%Dy^{3+},1 *at*%Tb^{3+}):YAG. The presence of the *f-d* bands of Tb^{3+} confirms that these states transfer energy to the Dy^{3+} ion (ETD_{fd} process in Fig. 8) as already observed in (3 *at*%Dy^{3+},0.5 *at*% Tb^{3+}):YAG. No other features ascribable to Tb^{3+} are observable, because too weak with respect to the Dy^{3+} bands.

The Dy^{3+} decay profiles of the co-doped samples excited at 447 nm (see Fig. 12) are strongly not exponential because of the presence of both Dy^{3+}-Dy^{3+} and Dy^{3+}-Tb^{3+} interactions. The decay times have then been estimated by integration of the normalized curves and the obtained values are reported in Table 1. The shorter decay time is expectedly that of the sample containing 5 *at*%Dy^{3+}, due to the concentration quenching whereas those of the 3 *at*%Dy^{3+} doped ceramics are very similar one to another (and to that of the singly doped sample), in line with their intensity behaviour.

Measurements carried out with excitation at 315 nm give rise to slower profiles, whose integrated decay times are reported in Table 1. This behaviour has already been accounted for previously in the (3 *at*% Dy, 0.5 *at*%Tb):YAG case.

The emission spectra excited at 315 nm are reported in Fig. 13.

The intensity increases as the concentration of Tb^{3+} increases from *0.5%at* to *1%at*, then decreases when the concentration of Dy^{3+} increases from *3%at* to *5%at*. This is an indication of the energy transfer

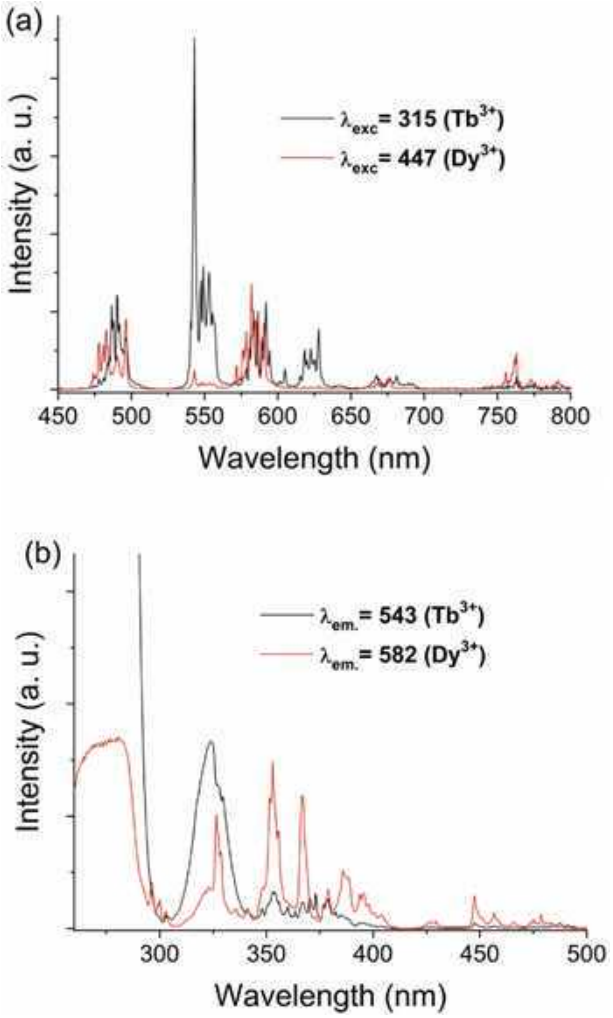


Fig. 7. (a) Emission spectra measured upon excitation at $\lambda_{exc} = 315$ (*f-d* Tb^{3+} transitions) and $\lambda_{exc} = 447$ nm (*f-f* Dy^{3+} transitions); (b) Excitation spectra of the 543 nm Tb^{3+} emission line and of the 582 nm Dy^{3+} emission line.

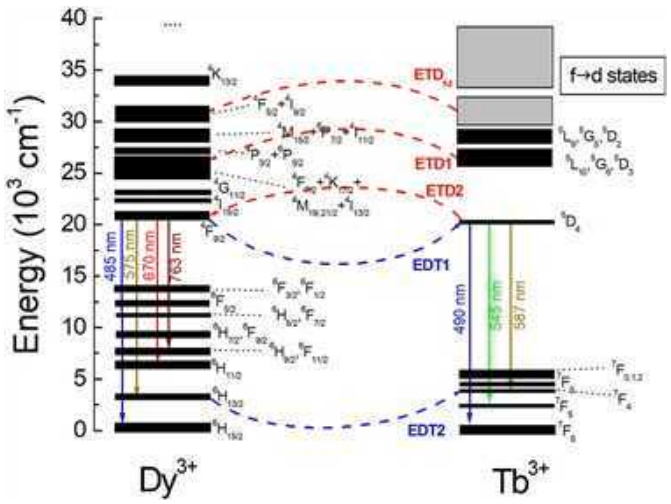


Fig. 8. Energy levels scheme showing the energy transfer processes between Dy^{3+} and Tb^{3+}.

from Tb^{3+} to Dy^{3+}, even if the spectra do not show clear signs of dysprosium emission. Only a careful examination of the structures of the

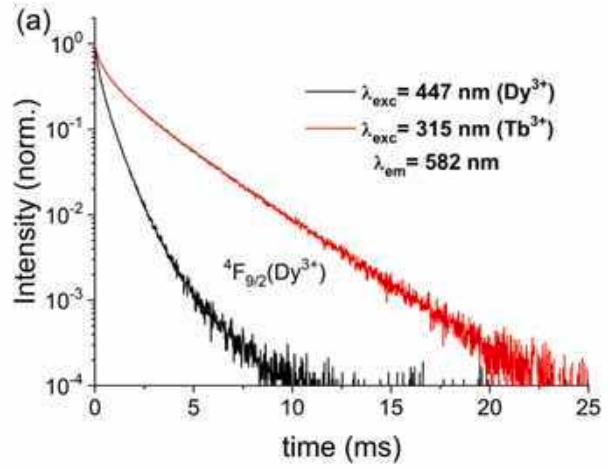


Fig. 9. (a) Emission decay profiles of Dy^{3+} $^4F_{9/2}$; (b) Tb^{3+} $^5D_4$.

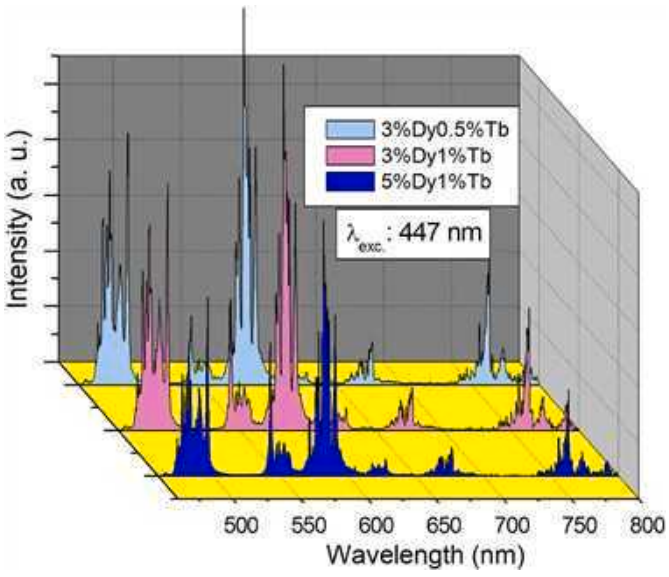


Fig. 10. Emission spectra of the ceramics measured upon Dy^{3+} excitation.

manifolds reveals some rather weak peaks around 572 and 763 nm, attributable to Dy^{3+}.

The decay profiles of the $^5D_4$ level, directly excited at 315 nm, are

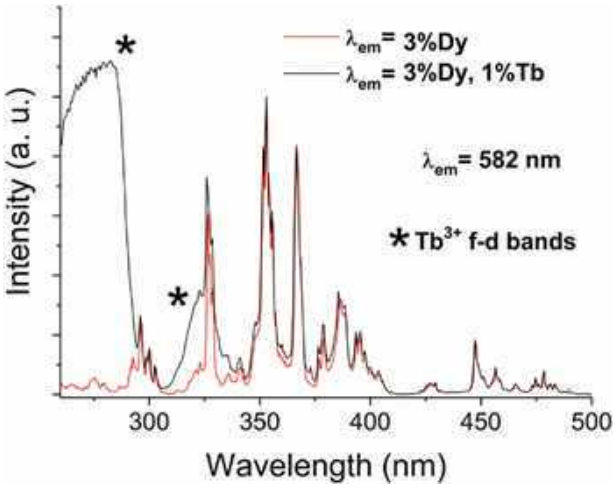


Fig. 11. Excitation spectra of the Dy^{3+} emission of 3 *at%*Dy:YAG and (3 *at%*Dy, 1 *at%*Tb):YAG. The spectra are normalized at 353 nm.

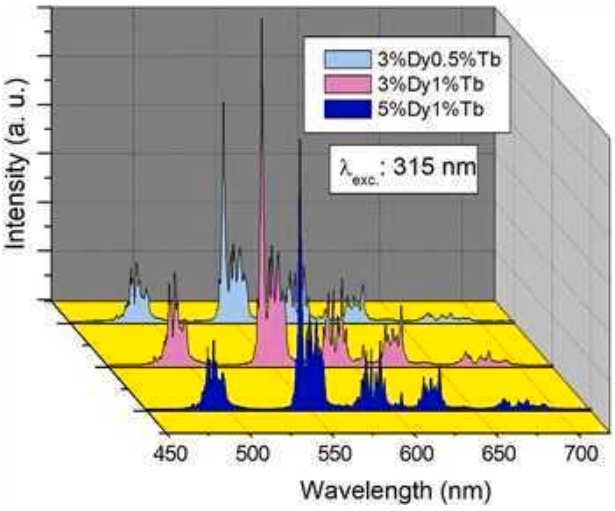


Fig. 13. Emission spectra of the ceramics measured upon Tb^{3+} excitation.

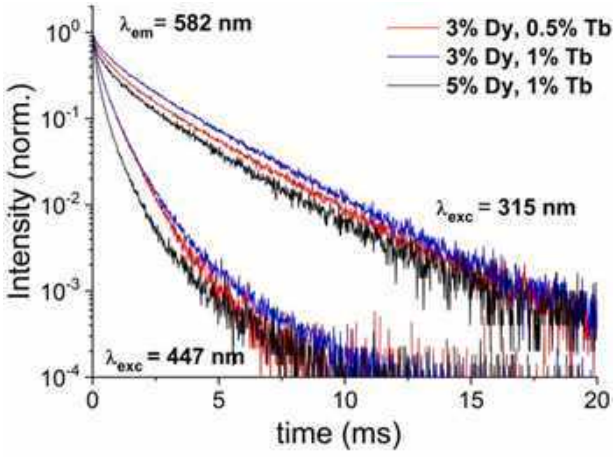


Fig. 12. Dy^{3+} emission decay profiles of all ceramic samples.

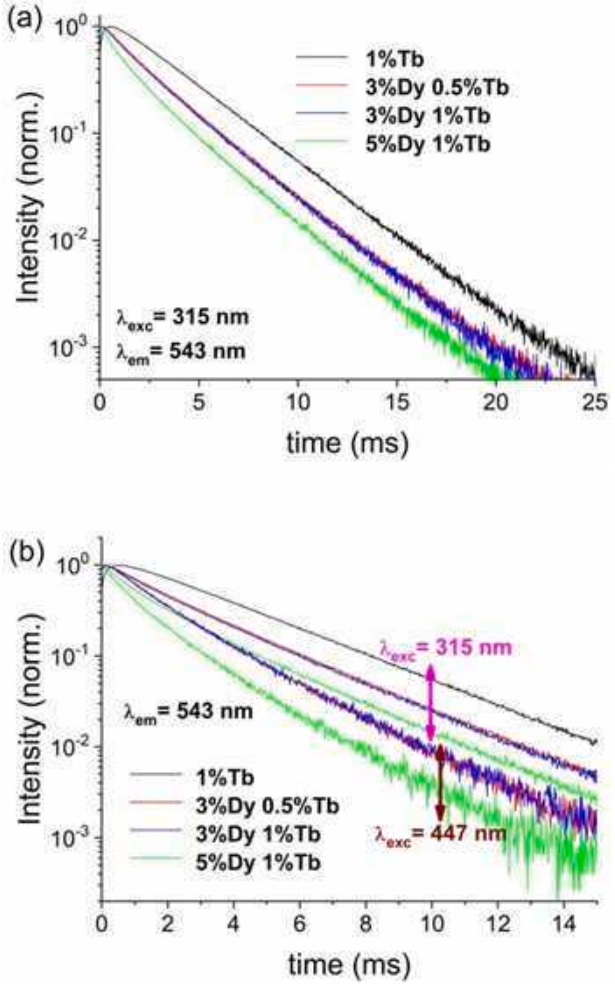


Fig. 14. (a) Tb^{3+} emission decay profiles at 543 nm, excited at 315 nm; (b) Comparison between the $^5D_4$ emission decay profiles excited at 315 nm and at 447 nm. The continuous lines represent the double exponential fit of the experimental data measured with 447 nm excitation.

Table 1
Decay times of the Dy^{3+} emission.

Sample	τ_{447} (ms)	τ_{315} (ms)
3 *at%*Dy	0.35	n.d
3 *at%*Dy, 0.5 *at%*Tb	0.36	1.13
3 *at%*Dy, 1 *at%*Tb	0.38	1.41
5 *at%*Dy, 1 *at%*Tb	0.25	0.94

compared in Fig. 14(a) with that of 1 *at%*Tb:YAG.

The samples containing *3%at.* of Dy still present a rise time, but it is very short, and the decay times, evaluated using Eq. (5), are similar. These results are summarized in Table 2. The (5 *at%*Dy^{3+}, 1.%Tb^{3+}): YAG ceramic has a shorter decay time, without any rise time.

The shortening of the rise time indicates a decrease of the $^5D_3$-$^5D_4$ cross relaxation efficiency, probably connected to the previously pointed out energy transfer from the $^5D_3$ level to the $^4P_{3/2}$, $^6P_{5/2}$ levels of the Dy^{3+} ions (see ETD1 in Fig. 8). The decrease of the $^5D_4$ decay time can be accounted for through a back transfer process from this state to the $^4F_{9/2}$ level of Dy^{3+} indicated as ETD2 in Fig. 8.

The 543 nm emission curves at were also recorded with excitation at 447 nm (see Fig. 14(b)): at this wavelength only the $^4F_{9/2}$ level of Dy^{3+} can be populated, and the Tb^{3+} emission originates from the (Dy^{3+}) $^4F_{9/2}$→(Tb^{3+}) $^5D_4$ energy transfer (EDT1 in Fig. 8). The curves present rise times practically identical to those evaluated with 315 nm excitation, but for the rest their behaviour is rather different. The descending part of the curves is faster, whereas at longer times they run parallel to those

Table 2
Decay and rise times, in ms, of the $^5D_4$ level of Tb^{3+}. The decay times reported for the curves measured with 447 nm excitation have been evaluated using Eq. (6).

Sample	τ_{dec} ($\lambda_{exc.}$ = 315 nm)	τ_{rise} (ms)	τ_1 ($\lambda_{exc.}$ = 447 nm)	τ_2 ($\lambda_{exc.}$ = 447 nm)
3 *at*%Dy	3.24	0.25	n. d.	n. d.
3 *at*%Dy, 0.5 at% Tb	2.53	0.03	1.30	2.54
3 *at*%Dy, 1 *at*%Tb	2.49	0.03	1.38	2.67
5 *at*%Dy, 1 *at*%Tb	1.93	n.d.	0.66	1.91

obtained by direct excitation. We have analysed the decays using a double exponential model (Eq. (6)):

$$\phi(t) = A_1 \cdot \exp\left(-\frac{t}{\tau_1}\right) + A_2 \cdot \exp\left(-\frac{t}{\tau_2}\right) \quad (6)$$

The results of the fits are reported in Table 2, where it is evident that for long times (above about 5 ms) the decays have the same trends, whereas at short times there is a mechanism that significantly increases the emission rate of the $^5D_4$ level, and that strongly depends on the Dy^{3+} concentration. We retain that this mechanism could consist in the (Tb^{3+}) $^5D_4 \rightarrow$ (Dy^{3+}) $^4F_{9/2}$ back transfer (see ETD2 in Fig. 8), whose efficiency has been previously pointed out.

3.3. (xat.%Dy, yat.%Tb):YAG crystals with (x = 3, 5; y = 0.5, 1)

The emission spectra of the crystals, excited at 447 nm, are shown in Fig. 15. As in the case of the ceramics, transfer towards Tb^{3+} is observed. This also appears to influence the total emission intensity, since the spectrum of the crystal most diluted in Tb^{3+} is the most intense. The intensity of the more concentrated crystal is conditioned by the interactions of the active ions. The excitation spectra (see Fig. 16) confirm that the $Tb^{3+} \rightarrow Dy^{3+}$ energy transfer occurs through excitation into the *f-d* states of Tb^{3+}.

The spectra evidence a stronger dependence of the intensity on the Dy^{3+} and Tb^{3+} concentrations with respect to the ceramics, indicating that the energy transfer processes are more efficient at long range, probably in consequence of the crystal ordering and of the absence of grain boundaries. The relative intensities obviously reflect those observed in emission. The only difference with respect to the analogous spectra of the ceramics lies in the better resolution of the high energy *f-d* transition, connected with the higher crystal ordering.

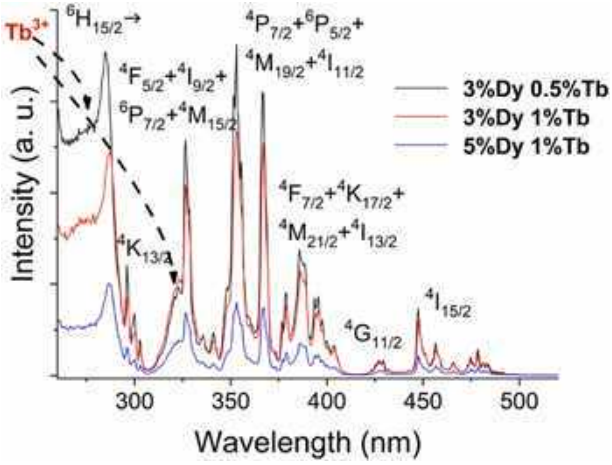


Fig. 16. Excitation spectra of the Dy^{3+} emission in the crystals.

The decay profiles of the Dy^{3+} visible emission are reported in Fig. 17. As in the ceramic case, they are strongly non-exponential. The decay times evaluated by integration of the normalized curves are reported in Table 3 and are very similar to those of the ceramics (see Table 1) confirming the quality of the latter.

The emission spectra excited at 315 nm are shown in Fig. 18. As in the case of the Dy^{3+} spectra, the intensity dependence on the doping levels is a bit higher than in the ceramics, for the reasons pointed out above. As previously, no bands attributable to Dy^{3+} are observable.

The excitation spectra (see Fig. 19) obviously reflect the trend of the emission spectra again with a more accentuated resolution of the main *f-d* band. The assignment has already been reported in Fig. 6(b).

The decay curves of the $^5D_4$ level, excited at 315 nm, are shown in Fig. 20. The average lifetimes of the 3 *at*%Dy doped samples are slightly longer than those of the corresponding transparent ceramics, while they remain identical for the 5 *at*%Dy sample. The decay times of the Tb^{3+} emission are summarized in Table 4.

Overall, the spectroscopic properties of the two series, ceramics and crystals, exhibit good agreement, except for some limited differences ascribable to the different crystallinity levels and, probably, to traces of extra-phases in the transparent ceramics.

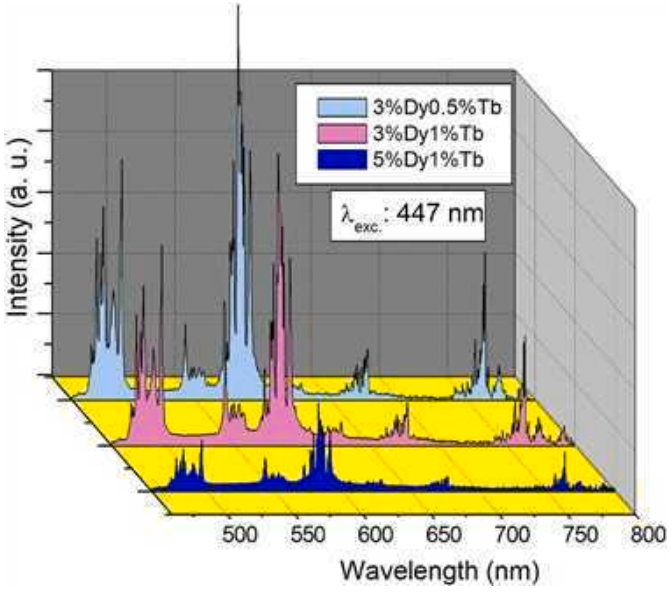


Fig. 15. Emission spectra of the crystals measured upon Dy^{3+} excitation.

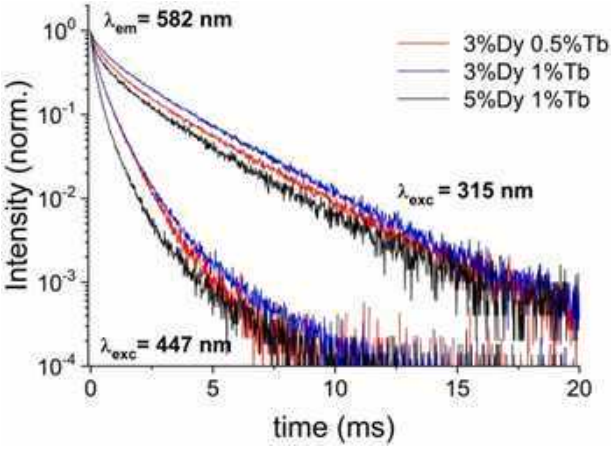


Fig. 17. Dy^{3+} emission decay profiles in the crystals.

Table 3
Decay times of the Dy^{3+} emission.

Sample	τ_{447} (ms)	τ_{315} (ms)
3 *at*%Dy, 0.5 *at*%Tb	0.38	1.27
3 *at*%Dy, 1 *at*%Tb	0.39	1.55
5 *at*%Dy, 1 *at*%Tb	0.24	1.03

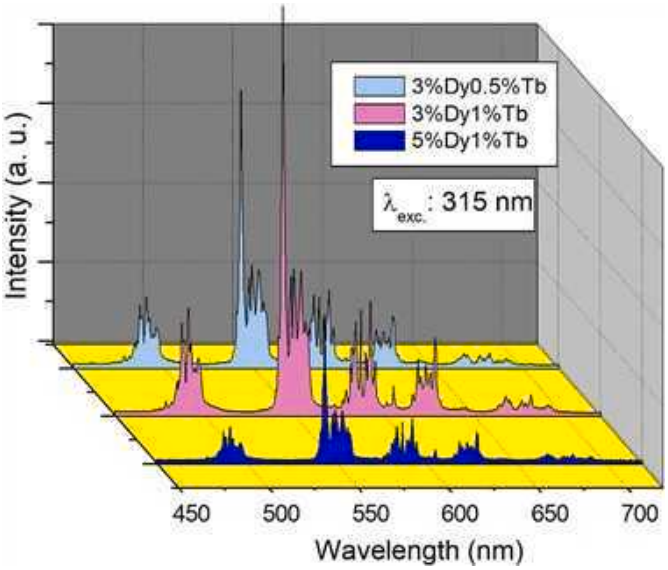


Fig. 18. Emission spectra of the crystals measured upon Tb^{3+} excitation.

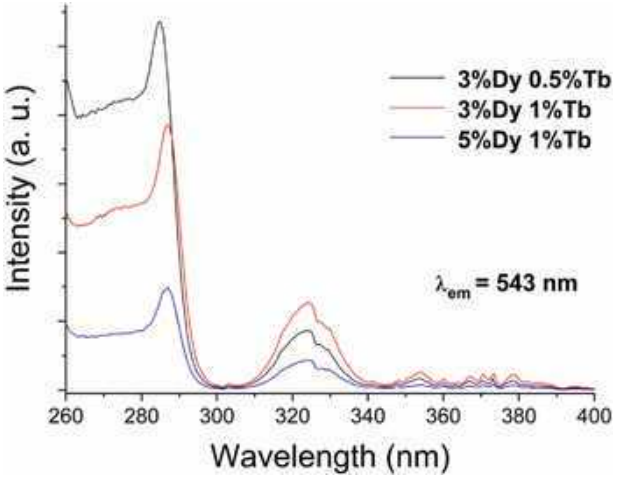


Fig. 19. Excitation spectra of the Tb^{3+} emission in the crystals.

4. Conclusions

An investigation has been carried out on the emission dynamics of high-quality Dy^{3+} and/or Tb^{3+} doped YAG transparent ceramics as well as of μ-PD grown single crystals with similar compositions. Steady-state and pulsed-light measurements have been carried out at room temperature in different experimental conditions, to identify the interaction processes between the doping ions that could have an impact on the population or depopulation of the potential visible lasing levels ($^4F_{9/2}$ of Dy^{3+} and $^5D_4$ and $^5D_3$ of Tb^{3+}). The emission spectra provide evidence of both $Tb^{3+}\rightarrow Dy^{3+}$ and $Dy^{3+}\rightarrow Tb^{3+}$ energy transfer processes, depending on the excitation conditions. The decay profiles evidence the role of the Dy^{3+} ion, connected to its relatively high concentration in the examined

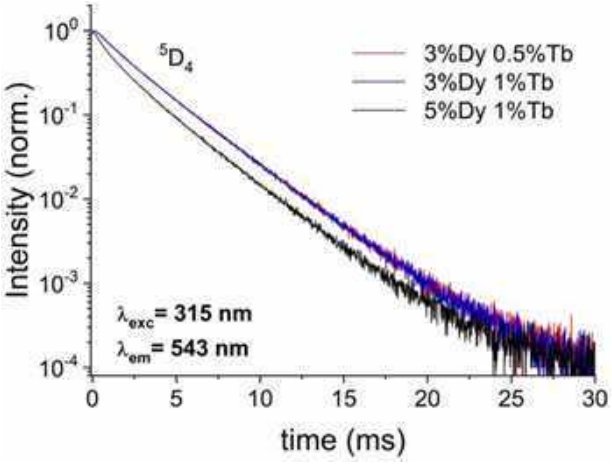


Fig. 20. Decay profiles of the $^5D_4$ emission of Tb^{3+} in the crystals.

Table 4
Decay times of the Tb^{3+} emission.

Sample	τ (ms)
3 *at*%Dy, 0.5 *at*%Tb	2.70
3 *at*%Dy, 1 *at*%Tb	2.67
5 *at*%Dy, 1 *at*%Tb	1.94

samples (3 and 5%), both in general and with respect to that of Tb^{3+}, in the emission processes.

The similarity of behavior of ceramics and crystals, apart some minor differences due to the different microstructures, is a clear evidence of the high quality of the transparent ceramics.

We consider the studied materials of potential interest for laser applications, and the provided information useful for determining the best composition for the realization of efficient visible emitting systems.

Funding

LAG Acknowledges financial contribution from the program EuPRAXIA Preparatory Phase (No.101079773)

CRediT authorship contribution statement

Angela Pirri: Conceptualization, Formal analysis, Investigation, Writing – original draft. **Andrea Lapini:** Investigation. **Jiang Li:** Investigation, Resources, Validation, Writing – review & editing. **Tingsong Li:** Resources. **Lexiang Wu:** Resources. **Yiyang Liu:** Resources. **Martin Nikl:** Resources, Validation, Writing – review & editing. **Jan Pejchal:** Resources. **Akira Yoshikawa:** Resources. **Guido Toci:** Validation, Writing – review & editing. **Leonida A. Gizzi:** Funding acquisition, Writing – review & editing. **Enrico Cavalli:** Formal analysis, Investigation, Methodology, Supervision, Writing – original draft.

Declaration of competing interest

The authors declare that they have no known competing financial interests or personal relationships that could have appeared to influence the work reported in this paper.

Acknowledgment

This work has benefited from the equipment and framework of the COMP-R initiative, funded by the 'Departments of Excellence' program of the Italian Ministry for University and Research (MUR, 2023-2027). The work is supported by Operational Programme Johannes Amos

Comenius financed by European Structural and Investment Funds and the Czech Ministry of Education, Youth and Sports (Project No. LASCIMAT– CZ.02.01.01/00/23_020/0008525).

Data availability

Data will be made available on request.

References

[1] C. Kränkel, D.T. Marzahl, F. Moglia, G. Huber, P.W. Metz, Laser Photon. Rev. 10 (2016) 548–568, https://doi.org/10.1002/lpor.201500312.
[2] Y. Cai, J. Ding, Z. Bai, Y. Qi, Y. Wang, Z. Lu, Opt. Laser Technol. 152 (2022) 108113, https://doi.org/10.1016/j.optlastec.2022.108113.
[3] J. Demaimay, P. Loiko, E. Kifle, F. Pau, G. Recoque, A. Benayad, T. Georges, P. Camy, A. Braud, Opt. Express 33 (2025) 9412–9422, https://doi.org/10.1364/OE.549247.
[4] Y. Kaneda, H. Tanaka, V. Temyanko, Opt. Express 33 (2025) 8903–8910, https://doi.org/10.1364/OE.549641.
[5] Y. Han, K. Guo, Y. Zhao, M. Xiong, D. Wang, J. Chen, X. Cui, B. Xu, Opt. Lett. 49 (2024) 3854–3857, https://doi.org/10.1364/OL.529272.
[6] D. Baiocco, I. Lopez-Quintas, J.R. Vázquez de Aldana, A. di Maggio, F. Pozzi, M. Tonelli, A. Tredicucci, Opt. Laser Technol. 186 (2025) 112628, https://doi.org/10.1016/j.optlastec.2024.112628.
[7] X.Y. Cai, Y. Wang, J.F. Li, et al., J. Lumin. 231 (2021) 117711, https://doi.org/10.1016/j.jlumin.2020.117711.
[8] Y. Huang, Y. Li, S. Pan, F. Yuan, L. Liu, L. Zhang, B. Li, Z. Lin, Opt. Laser Technol. 183 (2025) 112393, https://doi.org/10.1016/j.optlastec.2024.112393.
[9] X. Zhang, F. Meng, W. Li, S.I. Kim, Y.M. Yu, H.J. Seo, J. Alloys Compd. 578 (2013) 72–76, https://doi.org/10.1016/j.jallcom.2013.05.022.
[10] F. Peng, W. Liu, J. Luo, Y. Chen, H. Zhang, S. Ding, Q. Zhang, CrystEngComm 20 (2018) 6291–6301, https://doi.org/10.1039/C8CE01362D.
[11] S. Ding, H. Li, Q. Zhang, W. Liu, J. Lumin. 237 (2021) 118174, https://doi.org/10.1016/j.jlumin.2021.118174.
[12] R. Huang, P. Zhang, X. Huang, R. Wang, S. Zhu, H. Yin, Z. Chen, Opt. Mater. Express 7 (2017) 3673–3679, https://doi.org/10.1364/OME.7.003673.
[13] G. Bolognesi, D. Parisi, D. Calonico, G.A. Costanzo, F. Levi, P.W. Metz, C. Kränkel, G. Huber, M. Tonelli, Opt. Lett. 39 (2014) 6628–6631, https://doi.org/10.1364/OL.39.006628.
[14] Y. Gong, Y. Wang, Z. Wang, Y. Sun, Y. Yu, J. Lumin. 266 (2024) 120267, https://doi.org/10.1016/j.jlumin.2023.120267.
[15] J. Huang, Y. Lin, X. Gong, Y. Huang, Y. Chen, Opt. Mater. 150 (2024) 115287, https://doi.org/10.1016/j.optmat.2024.115287.
[16] Q. Xu, L. Sun, B. Zhang, J. Li, J. Gao, C. Nie, X. Shi, S. Sun, B. Teng, Y. Zhang, D. Zhong, J. Alloys Compd. 996 (2024) 174855, https://doi.org/10.1016/j.jallcom.2024.174855.
[17] M. Grüne, S. Schweizer, Materials 16 (2023) 2596, https://doi.org/10.3390/ma16072596.
[18] A. Pirri, E. Cavalli, J. Li, E. Sani, L. Wu, Y. Jing, P. Matteini, M. Vannini, G. Toci, Opt. Express 33 (2025) 23767–23781, https://doi.org/10.1364/OE.556214.
[19] A. Yoshikawa, M. Nikl, G. Boulon, T. Fukuda, Opt. Mater. 30 (2007) 6–10, https://doi.org/10.1016/j.optmat.2006.10.030.
[20] A. Yoshikawa, V. Chani, MRS Bull. 34 (2009) 266–270, https://doi.org/10.1557/mrs2009.75.
[21] R. Zheng, J. Ding, Q. Zhang, B. Li, Z. Wang, C. Liu, P. Lv, K. Yu, W. Wei, J. Am. Ceram. Soc. 102 (2019) 3510–3516, https://doi.org/10.1111/jace.16209.
[22] M. Inokuti, F. Hirayama, J. Chem. Phys. 43 (1965) 1978–1989, https://doi.org/10.1063/1.1703247.
[23] W.F. van der Weg, ThJ.A. Popma, A.T. Vink, J. Appl. Phys. 57 (1985) 5450–5456, https://doi.org/10.1063/1.334827.
[24] X. Liu, J. Zhao, M. Ge, J. Chen, H. Wang, S. Ding, Q. Zhang, Opt. Mater. 106 (2020) 110001, https://doi.org/10.1016/j.optmat.2020.110001.
[25] E. Cavalli, Opt. Mater. X 1 (2019) 100014, https://doi.org/10.1016/j.omx.2019.100014.
[26] J.P. Van der Ziel, L. Kopf, L.G. Van Uitert, Phys. Rev. B 6 (1972) 615–623, https://doi.org/10.1103/PhysRevB.6.615.
[27] D.J. Robbins, B. Cockayne, B. Lent, J.L. Glasper, Solid State Commun. 20 (1976) 673–676, https://doi.org/10.1016/0038-1098(76)91131-0.
[28] Z. Xing, M. Lun, W. Wu, H. Song, A. Yao, X. Zhou, Y. Wang, B. Chu, W. Li, Q. He, G. He, Ceram. Int. 46 (2020) 8971–8978, https://doi.org/10.1016/j.ceramint.2019.12.141.
[29] N. Bodenschatz, R. Wannemacher, J. Heber, D. Mateika, J. Lumin. 47 (1991) 159–167, https://doi.org/10.1016/0022-2313(91)90001-C.